DOI: 10.1002/chem.200500923

A Pyrazolato-Bridged Dinuclear Platinum(II) Complex Induces Only Minor Distortions upon DNA-Binding

Stéphane Teletchéa,[a] Seiji Komeda,[b, c] Jan-Maarten Teuben,[b, d] Miguel-Angel Elizondo-Riojas,[a, e] Jan Reedijk,*[b] and Jiří Kozelka*[a]

Abstract: The cytotoxic, pyrazolato-bridged dinuclear platinum(II) complex $[(cis\text{-}\{Pt(NH_3)_2\})_2(\mu\text{-}OH)(\mu\text{-}pz)]^{2+}$ (pz = pyrazolate) has been found to cross-link two adjacent guanines of a double-stranded DNA decamer without destabilizing the duplex and without changing the directionality of the helix axis. A ^{1}H NMR study of the oligonucleotide d(CTCTG*G*TCTC)-d(GAGACCAGAG), cross-linked at the two G* guanines by $[(cis\text{-}\{Pt(NH_3)_2\})_2(\mu\text{-}pz)]^{3+}$, and molecular dynamics simulations of the explicitly solvated duplex were performed to characterize the structural details of the adduct. The dinuclear platinum cross-link unwinds the helix by approximately 15°, that is, to a similar extent as the widely used antitumor drug cisplatin, but, in contrast to the latter, induces no significant bend in the helix axis. The Watson–Crick base-pairing remains intact, and the melting temperature of the duplex is unaffected by the cross-link. The helical twist is considerably reduced between the two platinated bases, as becomes manifest in an unusually short sequential H1′–H1′ distance. This unwinding also affects the sugar ring of the guanosine in the 3′-position to the cross-link, which presents an N⇌S equilibrium. This is the first cytotoxic platinum complex that has been successfully designed by envisioning the structural consequences of its binding to DNA.

Keywords: antitumor agents · molecular modeling · NMR spectroscopy · oligonucleotides · platinum

Introduction

The structural distortion of DNA caused by the binding of cisplatin (*cis*-diamminedichloroplatinum(II)) is accepted to play a pivotal role in the mechanism of action of this widely used antitumor drug.[1,2] The clinical use of cisplatin is not only restricted by its toxicity, but also by resistance development and by the limited scope of cancers against which it is active.[3,4] Most of the cisplatin analogues that have been synthesized to overcome toxicity problems have a similar activity profile to cisplatin.[4–6]

The major cross-link formed when cisplatin reacts with DNA is the 1,2-d(GG)-intrastrand adduct.[7] The DNA in this adduct is locally distorted from normal B-DNA, and the duplex is bent by 55–78° towards the major groove.[8–14] This distorted Pt–DNA structure is specifically recognized by DNA recognition proteins, which likely mediate the cytotoxic activity of cisplatin.[15–17]

Recent research has focused on compounds that form different types of cross-links with DNA. For example, Farrell and co-workers[18,19] have reported various di- and trinuclear platinum complexes that possess antitumor activity in vitro and in vivo and are characterized by their lack of cross-resistance with cisplatin. These compounds produce different

[a] Dr. S. Teletchéa,[+] Dr. M.-A. Elizondo-Riojas, Dr. J. Kozelka
Laboratoire de Chimie et Biochimie Pharmacologiques et Toxicologiques, Université René Descartes, UMR 8601 CNRS
45, rue des Saints-Pères, 75270 Paris Cedex 06 (France)
Fax: (+33) 142-868-387
E-mail: jiri.kozelka@univ-paris5.fr

[b] Dr. S. Komeda,[+] Dr. J.-M. Teuben, Prof. J. Reedijk
Leiden Institute of Chemistry, Leiden University
Gorlaeus Laboratories, P.O. Box 9502
2300 RA Leiden (The Netherlands)
Fax: (+31) 71-527-4671
E-mail: reedijk@chem.leidenuniv.nl

[c] Dr. S. Komeda[+]
Present address: School of Chemistry and Biochemistry, Georgia Institute of Technology, 315 Ferst Drive, Atlanta, GA 30332 (USA)

[d] Dr. J.-M. Teuben
Present address: Atlantic Supply, Technical Advisor Fuels
Société des Pétroles Shell, 92708 Colombes Cedex (France)

[e] Dr. M.-A. Elizondo-Riojas
Present address: Centro Universitario Contra el Cancer (CUCC)
Hospital Universitario "Dr. José Eleuterio Gonzalez"
Universidad Autónoma de Nuevo León, Monterrey, N.L. (Mexico)

[+] These two authors contributed equally to the present work.

Supporting information for this article is available on the WWW under http://www.chemeurj.org/ or from the author.

kinds of DNA cross-links and the structures of their DNA adduct drugs are drastically different from the distortions induced by cisplatin.[20,21] These results suggest that different DNA binding modes have different biological effects, and thus confer different activity profiles to the drugs inducing them.

One conceivable strategy for the development of new antitumor complexes is based on attempts to diminish the bend angle induced by the cisplatin 1,2-d(GG) cross-link. Following this idea, Kozelka et al.[22] have synthesized dinuclear hydrazine-bridged complexes that are highly cytotoxic in vitro but have no activity in animal models. More promising compounds based on this strategy are the azolato-bridged dinuclear platinum complexes recently reported by Komeda et al.[23–25] In particular, the complex $[(cis\text{-}\{Pt(NH_3)_2\})_2(\mu\text{-}OH)(\mu\text{-}pz)]^{2+}$ (pz = pyrazolate, see Figure 1),

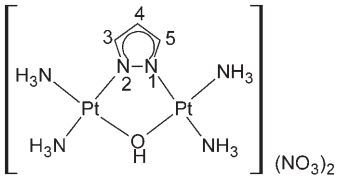

Figure 1. Structure of $[(cis\text{-}\{Pt(NH_3)_2\})_2(\mu\text{-}OH)(\mu\text{-}pz)](NO_3)_2$ (**1**). The numbering of the aromatic protons is indicated.

which features one pyrazolate and one hydroxide as bridging ligands, was shown to possess a cytotoxicity against MCF7 cells that is about 40 times higher than that of cisplatin; it is also active against cisplatin-resistant cells in vitro.[23]

The μ-hydroxide of $[(cis\text{-}\{Pt(NH_3)_2\})_2(\mu\text{-}OH)(\mu\text{-}pz)](NO_3)_2$ (**1**) acts as a leaving group, and the bridging rigid pyrazole keeps the correct distance between the two Pt atoms to enable binding of two neighboring guanines. This binding was illustrated in a recently reported crystal structure of the complex $[(cis\text{-}\{Pt(NH_3)_2\}(9\text{-Et-Gua}))_2(\mu\text{-}pz)]^{3+}$.[25] In this structure, the two 9-ethylguanines are stacked in a way which suggests that incorporation of such a cross-link into B-DNA would cause relatively minor distortions, in contrast to the 1,2-GG intrastrand cross-links formed by cisplatin. Thus, **1** is the first cytotoxic complex whose design rationale was based on envisioning a specific structural distortion caused upon binding to DNA, that is, avoiding a significant curvature of the DNA helix.

To carry out a detailed analysis of this distortion in a DNA duplex, we treated $[(cis\text{-}\{Pt(NH_3)_2\})_2(\mu\text{-}OH)(\mu\text{-}pz)]^{2+}$ with the decamer oligonucleotide d(CTCTGGTCTC) (ssI), and subsequently annealed the platinated single strand with its complementary strand d(GAGACCAGAG) (ssII). The resulting duplex containing the G-Pt-pz-Pt-G cross-link (dsII) was studied by high-resolution ^{1}H NMR spectroscopy and molecular dynamics (MD) simulations. The NOESY spectra of this platinated oligonucleotide differ only locally from the spectra of the unplatinated, undistorted duplex of the same sequence. The modeling work focused therefore on a precise characterization of the local distortion. To this end, we performed unrestrained MD simulations of the platinated duplex solvated in a periodic box of about 5000 water molecules. The trajectory of the MD simulation was then compared with the NMR spectroscopic data.

Results

Preparation and stability of the platinated DNA duplex: One major product is seen in the anion-exchange FPL chromatogram upon treatment of $[(cis\text{-}\{Pt(NH_3)_2\})_2(\mu\text{-}OH)(\mu\text{-}pz)](NO_3)_2$ with ssI at pH 4.0. The unplatinated ssI (charge −9) elutes at 11.00 min, and the newly formed platinated single strand (ssIII) containing the Pt-pz-Pt 1,2-intrastrand cross-link elutes at 9.02 min, in agreement with its reduced negative charge of −6. As in the case of the reactions with 9-ethylguanine[25]and 5′-GMP,[26] no intermediate species are observed. After three days the peak corresponding to ssI had almost completely disappeared and ssIII had formed in 90% yield. After titration of the complementary strand ssII (eluting at 10.57 min), the duplex d(CTCTG*G*TCTC)-d(GAGACCAGAG) (dsII; G* denotes a guanine involved in the Pt-pz-Pt cross-link) formed almost instantaneously (dsII elutes at 12.29 min).

T_m determination: An important measure of distortion is the melting temperature (T_m) of the platinated DNA compared to unplatinated DNA. The melting curves of dsI and dsII were determined under identical conditions (3.4×10^{-9} M in 1 M NaCl, 50 mM phosphate buffer, pH 7.0). The melting temperatures (49 ± 1 °C for the unplatinated dsI and 48 ± 1 °C for the platinated dsII) are identical within the error limits, and therefore it can be concluded that the DNA duplex is not significantly destabilized by binding of $[(cis\text{-}\{Pt(NH_3)_2\})_2(\mu\text{-}pz)]^{3+}$.

The duplex stability of the NMR sample of dsII (4 mM, 50 mM phosphate buffer pH 7.0, no additional NaCl added) was checked by NMR spectroscopy before conducting 2D experiments. All exchangeable protons remain visible until the duplex is heated to 293 K. At higher temperatures these signals broaden and at 323 K they disappear entirely. All subsequent NMR experiments were conducted at 283 K. At this temperature the sample is still in duplex conformation and overlap of the H3′ peaks with the H_2O peak is minimized. Both dsI and dsII were found to be stable for at least one week at ambient temperature.

NMR studies

Assignments of chemical shifts: The labeling of atoms and torsion angles in an oligonucleotide is defined in Figure 2. The combined use of TOCSY and NOESY spectroscopy allowed the assignment of the protons of dsI (the unplatinated duplex d(CTCTGGTCTC)-d(GAGACCAGAG)) and dsII.[27–29] The NOESY region (200-ms mixing time) of

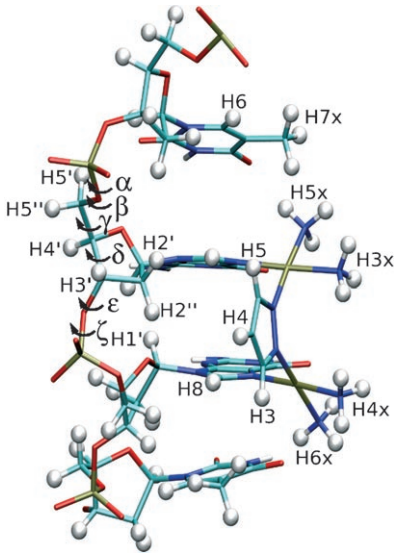

Figure 2. Labeling of atoms and torsion angles within the DNA tetranucleotide TGGT. Cross-linking of the two guanines by the Pt-pz-Pt residue is shown as well. This is a fragment of the structure shown later in Figure 7, and the picture serves to identify atoms in the central part of the platinated strand that are close in space and susceptible to give rise to NOE cross-peaks.

duplex dsII visualizing the cross-peaks of the pyrazole moiety is shown in Figure 3a, and the sequential assignment pathway of dsII is shown in Figure 3b.

The adenine H2 protons could easily be identified from their long relaxation times in the T1 relaxation experiment, and were assigned on the basis of intra-residue H2 to H1′ cross-peaks and sequential nH2, $(n+1)$H1′ contacts. The H2′ and H2″ sugar protons were assigned stereospecifically on the basis of the intensities of the H1′ to H2′/H2″ contacts.[30] No stereospecific assignments were obtained for H5′ and H5″. For the unplatinated dsI the H2, H5′, and H5″ protons were not assigned. The pyrazole protons (see Figure 1 for numbering) were assigned as follows: the H5 proton was assigned as being closest to G*5, that is, on the 5′ side of the Pt-pz-Pt lesion, H3 is directed towards the 3′ side, and H4 is the central proton. Figure 3a shows the cross-peaks of the H8/H6 protons with the three pyrazole protons. In the imino region of the ^{1}H NMR spectrum in H_2O all imino protons were identified (with the exception of those of the 3′ terminal G11), thus indicating that the Watson–Crick hydrogen bonding is conserved between the platinated bases. Each of these imino protons shows cross-peaks in the NOESY spectra in H_2O/D_2O. The chemical shifts of the nonexchangeable and exchangeable protons are listed in Table 1.

The plot of differential chemical shifts of the platinated dsII versus those of the unplatinated dsI (Figure 4) immediately revealed some intriguing differences. The presence of the Pt-pz-Pt complex shifts the resonances in the vicinity of the platinum lesion. The most striking of these is the *upfield* shift of the H8 protons of G*5 and G*6 as these protons are normally shifted *downfield* upon platinum coordination at the N7 atom because of the inductive effect of platinum binding.[31] This exceptional upfield shift of G*5 and G*6 can be explained by the position of the pyrazole in the major groove (vide infra). The protons of the bases T4 and G*5 exhibit larger differences in chemical shifts than those of G*6 and T7; the shift differences are minor for the other bases in the duplex. In fact, only minor differences are observed for the sugar protons of the two cytosines opposing the platinated guanines (C15 and C16), although the aromatic protons NH1 and NH2 of these bases are shifted significantly upfield upon platination. The NH1 protons shift by 1.08 and 1.53 ppm for C15 and C16, respectively, and the NH2 protons shift by 1.41 and 1.03 ppm (see Table 1).

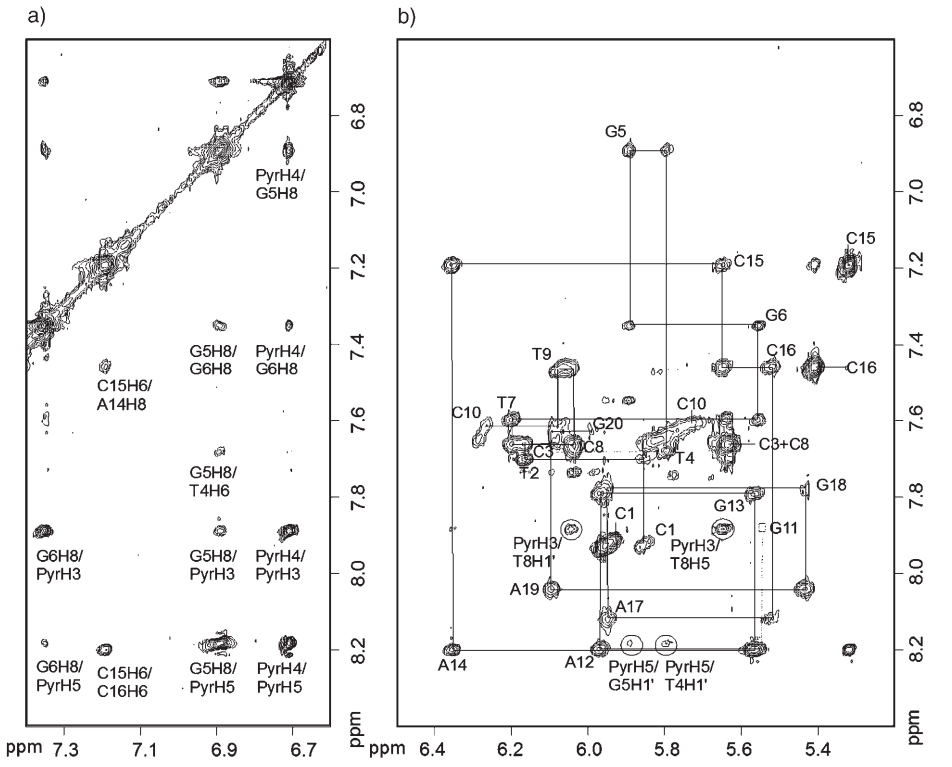

Figure 3. Contour plots of two regions of the 200-ms NOESY spectrum of duplex dsII. a) The region of the cross-peaks of the pyrazole protons. b) The H8/H6 to H1′/H5 region. The sequential assignment pathway for both strands is indicated. Assignments of cytidine H6/H5 cross-peaks are also indicated, and the pyrazole to DNA cross-peaks in this region are encircled.

Table 1. Chemical shifts [ppm] of the protons in dsI and dsII at 283 K.

	H8/H6	H2/H5/Me	H1′	H2′	H2″	H3′	H4′	NH1/NH2[a]	H1/H3
DsI									
C1	7.94	5.96	5.86	2.29	2.60	4.66	4.11	[b]	
T2	7.69	1.69	6.21	2.31	2.62	4.66	4.30		13.66
C3	7.65	5.65	6.05	2.13	2.53	4.84	4.20	8.34/7.02	
T4	7.53	1.66	5.67	2.04	2.40	4.85	4.12		13.90
G5	7.87		5.71	2.72	2.75	5.00	4.37		12.97
G6	7.53		5.61	2.21	2.54	[c]	4.14		12.80
T7	7.64	1.27	5.94	2.52	2.74	4.84	4.40		13.97
C8	7.62	5.61	6.02	2.16	2.53	4.77	4.77	8.40/7.09	
T9	7.63	1.71	6.10	2.18	2.53	[c]	4.17		14.06
C10	7.66	5.81	6.28	2.27	2.29	4.58	4.05	[b]	
G11	7.88		5.54	2.50	2.69	4.83	4.16		[b]
A12	8.19	[a]	5.97	2.75	2.88	5.06	4.40		
G13	7.72		5.55	2.59	2.71	5.01	4.39		12.65
A14	8.12	[a]	6.23	2.63	2.91	5.02	4.48		
C15	7.19	5.15	5.78	1.94	2.37	5.15	4.14	8.03/6.73	
C16	7.40	5.15	5.34	1.96	2.28	5.48	4.04	8.48/6.44	
A17	8.17	[a]	5.90	2.71	2.84	5.03	4.37		12.67
G18	7.74		5.38	2.57	2.66	4.98	4.33		
A19	8.05	[a]	6.11	2.61	2.90	5.01	4.42		13.36
G20	7.61		5.98	2.36	2.24	4.61	4.15		
DsII									
C1	7.93	5.96	5.86	2.29	2.60	4.65	4.11	7.21/5.97	
T2	7.71	1.67	6.17	2.39	2.59	4.65	4.30		13.94
C3	7.67	5.64	6.04	2.31	2.57	4.78	4.25	8.41/7.08	
T4	7.68	1.73	5.79	2.46	2.47	4.99	4.23		14.08
G*5	6.90		5.89	2.19	2.52	4.99	4.78		13.43
G*6	7.35		5.55	2.20	2.60	5.04	4.27		13.37
T7	7.60	1.18	6.20	2.29	2.65	4.88	4.32		13.70
C8	7.67	5.64	6.04	2.16	2.58	4.84	4.16	8.45/7.18	
T9	7.47	1.73	6.07	2.16	2.53	4.88	4.16		14.04
C10	7.65	5.83	6.28	2.27	2.28	4.59	4.06	8.30/7.24	
G11	7.88		5.57	2.53	2.69	4.83	4.17		[b]
A12	8.20	7.54	5.97	2.75	2.88	5.06	4.42		
G13	7.79		5.56	2.63	2.73	5.04	4.41		12.76
A14	8.20	7.89	6.36	2.70	3.04	5.04	4.54		
C15	7.19	5.32	5.65	1.92	2.41	4.74	4.11	6.95/5.32	
C16	7.46	5.41	5.52	2.03	2.34	4.83	4.11	6.95/5.41	
A17	8.12	7.79	5.95	2.71	2.83	5.03	4.35		
G18	7.77		5.44	2.59	2.70	5.00	4.35		12.62
A19	8.04	7.74	6.10	2.61	2.90	5.01	4.43		
G20	7.63		5.99	2.38	2.24	4.61	4.16		12.76

[a] NH1 is the proton involved in hydrogen bonding. [b] Not observed. G* denotes platination of the guanine. [c] Overlap with HDO peak.

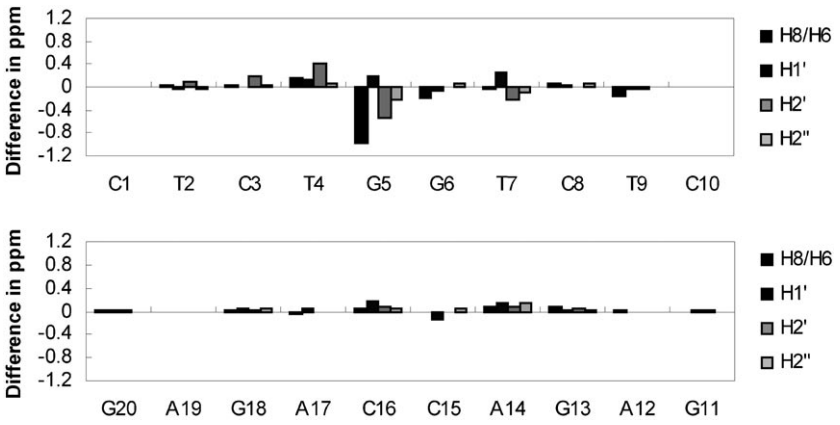

Figure 4. Differences in chemical shift upon platination (dsII-dsI).

NOESY spectra and T1 measurements: A comparison of the NOE intensities of dsII with those of the unplatinated dsI (Figure 5) confirmed the indication from the chemical shifts that the structural perturbation is limited to the close vicinity of the platinum complex. The most obvious difference is the appearance of drug–DNA contacts of the pyrazole ligand with the two central guanines. The intensities of these NOEs differ by factors of up to 30 and indicate that the G*5 base is closer to the pyrazole ring than G*6. The NOE intensities determined at a mixing time of 200 ms correlated well with the time average of the −6th power of the internuclear distance over the MD simulation (vide infra). The other NOE cross-peaks were classified as strong, medium, or weak and are summarized for the central parts of both the platinated (dsII) and unplatinated (dsI) duplexes in Figure 5. The most striking difference between dsI and dsII is that dsII exhibits an unusual H1′ to H1′ contact (medium intensity) between G*5 and G*6, thus indicating a decreased distance between these protons.

For G*6 we observe weaker intra-residue H2′–H8 and H2″–H8 NOEs, which indicate a shift of the conformational equilibrium of the deoxyribose towards a higher population of the N-type conformation. For the S-type conformation normally observed in B-DNA, the H8 to H2′/H2″ cross-peaks are strong in intensity, and they are also strong for G6 in dsI. Unfortunately, the G*6 H3′ proton resonates too close to the HDO peak in dsII to allow a reliable quantification of the H8 to H3′ cross-peak, thus no information on the sugar conformation could be derived from this NOE. However, another indication of an S-to-N repuckering

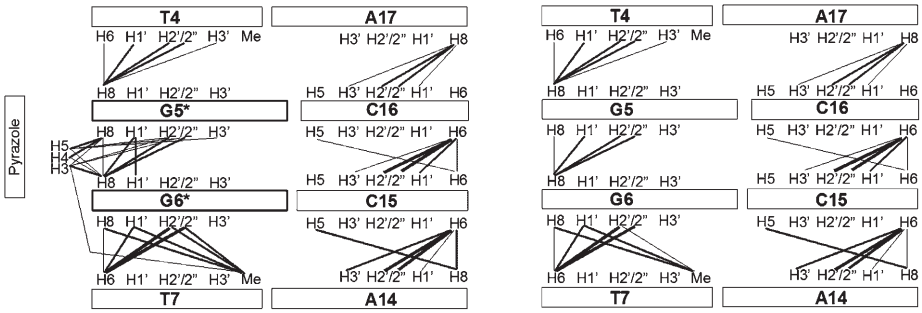

Figure 5. Schematic illustration of the internucleotide NOE cross-peaks in the platinated duplex dsII (left) and the unplatinated duplex dsI (right). The intensities are represented by the thickness of the lines denoting strong, medium, and weak cross-peaks.

of G*6 upon platination comes from spin-lattice relaxation measurements (Table 2), which show that the T1 value for the H8 proton of G*6 in dsII is about three times longer than for the other H8 protons. Since the most efficient pathway for H8 relaxation is over the H2′ proton,[32,33] the increase of the T1 of G*6H8 indicates a decrease of the interatomic H8–H2′ distance, as observed for an S→N transition. In contrast to G*6, there is no indication of a shifted conformational equilibrium for the other platinated base (G*5).

Table 2. Spin-lattice relaxation times (T1 values) of the H8/H6 protons of dsII at 283 K.

Res.	C1	T2	C3	T4	G*5	G*6	T7	C8	T9	C10
H8/H6 [ppm]	7.93	7.71	7.67	7.68	6.90	7.35	7.60	7.67	7.47	7.65
T1 [s]	1.8	[a]	1.5	1.0	1.0	3.5	1.0	1.5	1.0	1.0
Res.	G20	A19	G18	A17	C16	C15	A14	G13	A12	G11
H8/H6 [ppm]	7.63	8.04	7.77	8.12	7.46	7.19	8.20	7.79	8.20	7.88
T1 [s]	0.8	1.1	2.3[a]	0.8	1.0	[a]	[a]	2.3[a]	[a]	[a]

[a] Overlap of proton signals.

Another clear difference between the NOESY spectra of dsI and dsII involves the inter-residue cross-peaks between G*6 and T7: the cross-peaks connecting H2′ and H2″ of G*6 with the methyl group of T7 have medium intensity in dsII, whereas in dsI they are weak and almost invisible. Since the sequential H2′(n)–TCH$_3$(n+1) distance within B-DNA is largely independent of the sugar pucker on nucleotide n, the decrease of this distance must either be due to an approach between the G*6 deoxyribose and the T7 base or to a change in the glycosidic torsion angle χ of T7. The H2″(n)–TCH$_3$(n+1) distance, on the other hand, does depend on the sugar pucker of nucleotide n, and *increases* significantly when this nucleotide passes from S to N. The enhancement of the G*6H2″–T7CH$_3$ NOE upon platination thus argues against a pure N conformation of G*6.

Other differences in NOE intensities upon platination occur in C15 (nucleotide complementary to G*6). The intra-residue H6 to H3′ cross-peak increases from medium to strong intensity at the cost of the H6 to H2′/H2″ cross-peaks, which decrease in intensity from strong to medium; the intensity of the H6 to H1′ cross-peak, however, has a normal intensity. This observation indicates that the mean conformation of the sugar of C15 is also shifted towards a lower phase angle. For comparison, the distance between the H6 and H3′ protons is 2.8–3.0 Å for an N-type conformation and 4.0–4.4 Å for the S-type conformation that is normally seen in B-DNA.

Molecular dynamics simulations of solvated duplex dsII

A 20-ns molecular dynamics (MD) simulation of the platinated duplex dsII, explicitly solvated in water, was carried out as outlined in the Experimental Section. Since the above analysis of NMR spectroscopic data suggested that the nucleotides G*6 and C15 might show a dynamic S⇌N equilibrium, we were interested in the dynamic features of the structure. We therefore carried out unconstrained MD simulations of dsII, checked that they allowed the salient observations from the NMR spectra (including atypical chemical shifts, NOE intensities, and T1 values) to be rationalized, and used the MD simulation of dsII to predict its global structure. The NMR features of dsI were indicative of normal B-DNA. Our task was thus to find out how dsII deviates from the normal B-DNA double helix.

The main structural conclusions that one can draw from the comparison of the NMR spectra of dsI and dsII (vide supra) are:

1) the structural modifications due to the dinuclear platinum cross-link are limited to the base-pairs close to the cross-link;
2) the mean sugar phase-angles of both G*6 and C15 pass from overwhelmingly S to intermediate between N and S upon platination;
3) the T7 base seems to be "pushed" closer to the sugar of G*6 by the cross-link;
4) the pyrazole moiety is somewhat closer to G*5 than to G*6.

All these features are reproduced by the dynamic models, as described in the next paragraphs. The MD trajectories were analyzed using plots of structural parameters (dihedral angles, helicoidal parameters) as a function of time (see Figure S1 for the complete list). The evolution of deoxyribose

phase-angles and of the helicoidal parameters twist and roll of the four inner base-pairs is shown in Figure 6. The mean values of twist and roll, with standard deviations, are compared to those of the non-platinated duplex in Table 3.

Different effects of the Pt-pz-Pt cross-link on sugar puckers of G*6 and C15: It can be seen from Figure 6 that the sugar pucker of G*6 undergoes well-defined transitions between N- and S-type conformations. The NMR spectroscopic data (vide supra) have indicated that G*6 presents an N⇌S equilibrium, and the MD simulation is in agreement with this observation. On the other hand, G*5 keeps its S-type pucker, which is also in agreement with the NMR spectroscopic data. This agreement indicates that our parameterization of the sugar pucker of the platinated guanosines (see Experimental Section) is correct. We recall that these sugar puckers reflect both an inductive effect of platinum binding to guanine (favoring N-pucker[34–38]) and steric effects. Whereas the former is supposed to affect both guanosines equally (and the force-field parameters applied to both platinated guanosines were thus identical), the latter are obviously different, and it is this difference in the steric effects that causes the puckers of G*5 and G*6 to be different. The sub-populations of snapshots having either N- or S-pucker on G*6 were averaged and energy-minimized. The resulting model with G*6N is shown in Figure 7.

The NMR spectroscopic data also indicate that, in addition to G*6, the cytidine complementary to G*6, C15, also undergoes a change of its sugar conformation upon platination. In the platinated duplex dsII this nucleotide shows increased intra-nucleotide H2′–H6 and H2″–H6 distances and a decreased H3′–H6 distance. In the framework of the classical two-state N/S model,[39] such changes would be interpreted as indicating a shift of the N⇌S equilibrium towards N. However, the MD simulation showed that C15 assumes an E-type pucker (Est, O4′-*endo*, $60° < P < 120°$)[40]. This conformation, which is characterized by a phase angle of around 100°, remained stable during the whole simulation, with only a few excursions to S (Figure 6). Thus, the unwinding of the double helix imposed by the GG cross-link shifts the mean phase-angle of both G*6 and C15 towards lower values, but, as the MD simulation indicates, in two different ways: for G*6, by making transitions from S to N more frequent, and for C15, by constraining it to an E conformation. The reason for this difference could reside in different stabilities of the E conformation in purine versus pyrimidine nucleotides with respect to N and S. In fact, analysis of the high-resolution (better than 2 Å) crystal structures extracted from the Nucleic Acids Data Bank, using the selection criteria described by Djuranovic and Hartmann,[40] revealed that of the selected 155 AT base-pairs, 6% of the adenosines and 28% of the thymidines have an E-type pucker, and of the 233 selected GC pairs, 14% of the guanosines and 22% of the cytidines have an E pucker (E-pucker was defined as $60° < P < 120°$). Thus, for pyrimidine nucleotides the E-pucker domain seems more readily accessible (i.e., energetically less unfavorable) than for purine nucleotides.

The Pt-pz-Pt cross-link unwinds the GpG dinucleotide but does not introduce a significant bend: It can be seen from Figure 7 that the platinated duplex dsII does not show significant bending. This is also corroborated by the values of roll (Table 3), which do not change significantly upon platination. On the other hand, the approach of the N7 atoms necessary for the formation of the cross-link causes significant unwinding (diminution of twist) of the cross-linked step G*5:C16/G*6:C15. As seen in Figure 6c and Table 3, this step is unwound from about 36° to about 23°. In the NOESY spectra, this unwinding is reflected by the appearance of the medium intensity G*5H1′–G*6H1′ NOE. This distance is observed to be 5.1 ± 0.5 Å in the simulation of dsI (not shown), and decreases to 3.2 ± 0.4 Å upon platination. The sugar pucker of G*6 has a significant influence on this distance: the values observed in the time-averaged models are 2.83 and 3.32 Å for N- and S-pucker on G*6, respectively, as can be seen from the detailed views presented in Figure 8. This provides a supplementary argument against a pure N-conformation of G*6, since for a distance of 2.8 Å a strong NOE would be expected instead of the observed medium NOE. Table 3 suggests that the unwinding of the G*5:C16/G*6:C15 step is partly compensated by a slight overwinding of the G*6:C15/T7:A14 step with respect to the unplatinated duplex. This overwinding is most probably the principal origin of the increase of the intensity of the G*6H2′–T7CH$_3$ NOE. The time averages of the G*6H2′–T7C7 distance are 3.6 ± 0.4 Å in dsI and 3.3 ± 0.3 Å in dsII.

Perusal of the backbone torsion angles (Figure S1 in the Supporting Information) shows that the GpG step assumes the non-canonical $\alpha^-\beta^+\gamma^t$ conformation during the whole simulation. This conformational sub-state is occasionally found in protein–DNA complexes and is characterized by particularly low twist ($27.4 \pm 0.5°$ as compared to $31.4 \pm 0.9°$ for the canonical $\alpha^-\beta^t\gamma^+$ conformation).[43] Our simulations indicate that this "strategy" that DNA uses in protein-bound structures to facilitate the unwinding needed for protein recognition is also utilized here to accommodate the unwinding imposed by the covalent cross-link with the dinuclear platinum complex.

Contacts between the platinum ligands and DNA: As can be seen from Figure 8, the orientation of the guanine with respect to the platinum coordination plane is non-orthogonal at both platinum centers; therefore, hydrogen bonds between the NH$_3$ ligand *trans* to pyrazole and the guanine O6 atom are possible. These N–H···O6 hydrogen bonds were found to persist during the whole simulation, the average N···O separations being 2.90 ± 0.12 and 2.96 ± 0.13 Å for G*5 and G*6, respectively. Moreover, each of these NH$_3$ ligands was found to form an additional hydrogen bond to the O4 atom of the neighboring thymine, i.e., T4 with the 5′-NH$_3$ (3.16 ± 0.26 Å) and T7 with the 3′-NH$_3$ (3.07 ± 0.17 Å). Thus, each NH$_3$ ligand simultaneously makes one hydrogen bond with the proximate guanine and another with the adjacent thymine: 5′-NH$_3$ forms one quasi-linear (N–H···O angle of about 170°) and one bifurcated hydrogen

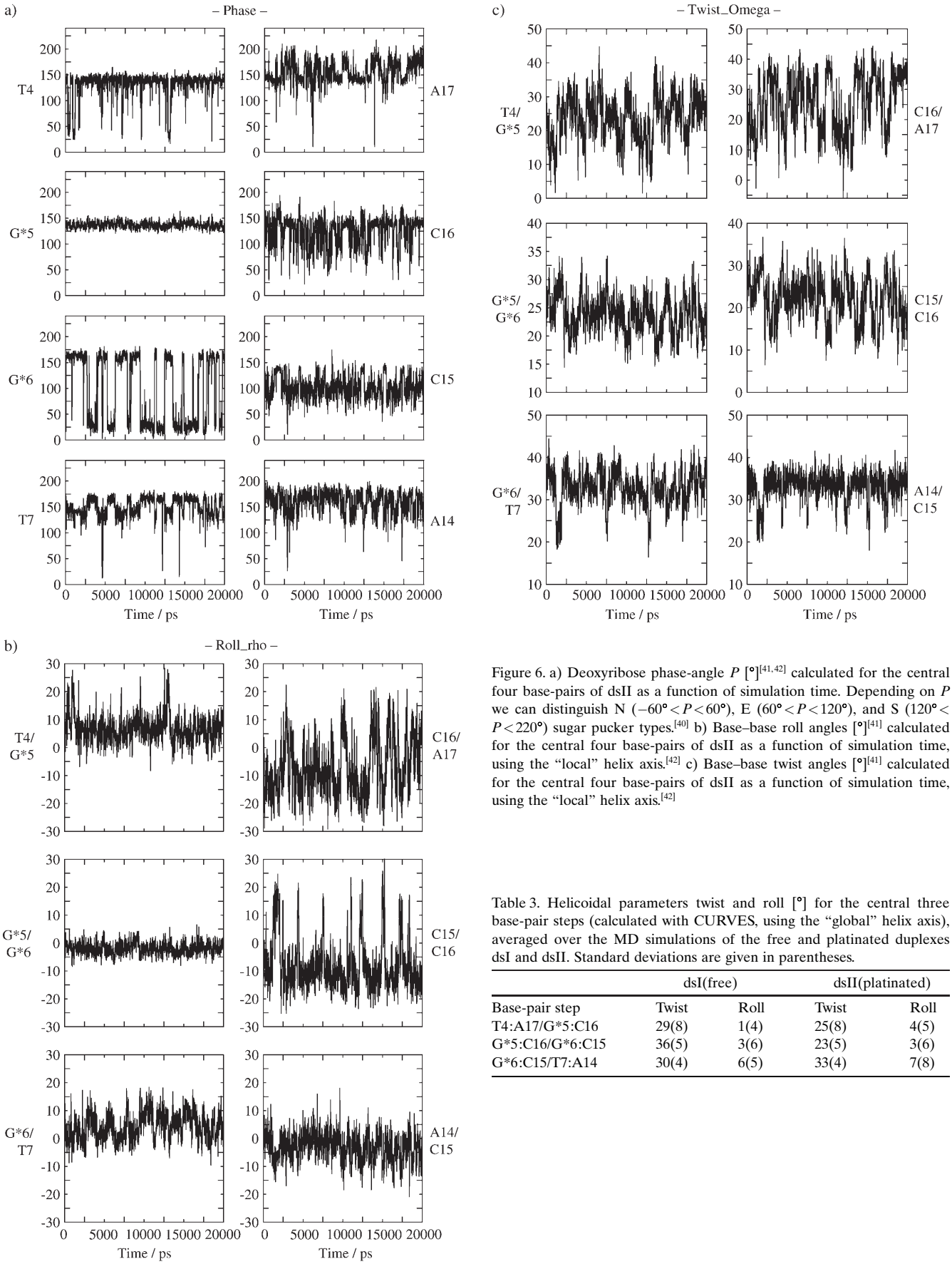

Figure 6. a) Deoxyribose phase-angle P [°][41,42] calculated for the central four base-pairs of dsII as a function of simulation time. Depending on P we can distinguish N ($-60° < P < 60°$), E ($60° < P < 120°$), and S ($120° < P < 220°$) sugar pucker types.[40] b) Base–base roll angles [°][41] calculated for the central four base-pairs of dsII as a function of simulation time, using the "local" helix axis.[42] c) Base–base twist angles [°][41] calculated for the central four base-pairs of dsII as a function of simulation time, using the "local" helix axis.[42]

Table 3. Helicoidal parameters twist and roll [°] for the central three base-pair steps (calculated with CURVES, using the "global" helix axis), averaged over the MD simulations of the free and platinated duplexes dsI and dsII. Standard deviations are given in parentheses.

	dsI(free)		dsII(platinated)	
Base-pair step	Twist	Roll	Twist	Roll
T4:A17/G*5:C16	29(8)	1(4)	25(8)	4(5)
G*5:C16/G*6:C15	36(5)	3(6)	23(5)	3(6)
G*6:C15/T7:A14	30(4)	6(5)	33(4)	7(8)

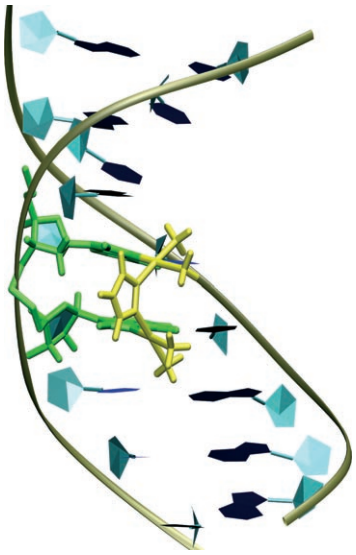

Figure 7. One of the two main conformations observed during the MD simulation of dsII. This model was obtained by averaging the snapshots having the G*6 sugar in an N-type conformation and energy minimization, as described in the Experimental Section. The platinated G*pG* dinucleotide is shown in green and the {*cis*-[Pt(NH_3)$_2$]}$_2$(μ-pz)$^{3+}$ residue in yellow.

bond, whereas 3′-NH_3 forms two bifurcated hydrogen bonds. The exchange between hydrogen atom positions that we observe is relatively rapid (~10^8 s^{-1}). We have no experimental evidence for these hydrogen bonds; however, their presence is closely related to the position of the pyrazole residue, for which we have the experimental check with six NOE distances (vide infra).

The NOESY spectra show six contacts between the pyrazole C-H protons and the sugar protons of the adjacent residues (G*5, G*6). The NOE intensities determined at a 200-ms mixing time are listed in Table 4 together with the corresponding H–H distances time-averaged over the MD simulation. Also given are distances determined from the NOE intensities (I_{NOE}) as $(c/I_{NOE})^{1/6}$, with c taken as 25000. The excellent agreement between these calculated and NOE-derived values suggests that the platinum binding-site is portrayed very well by the simulation. The shorter distances determined for G*5 indicate that the pyrazolate moiety is closer to this base than to G*6.

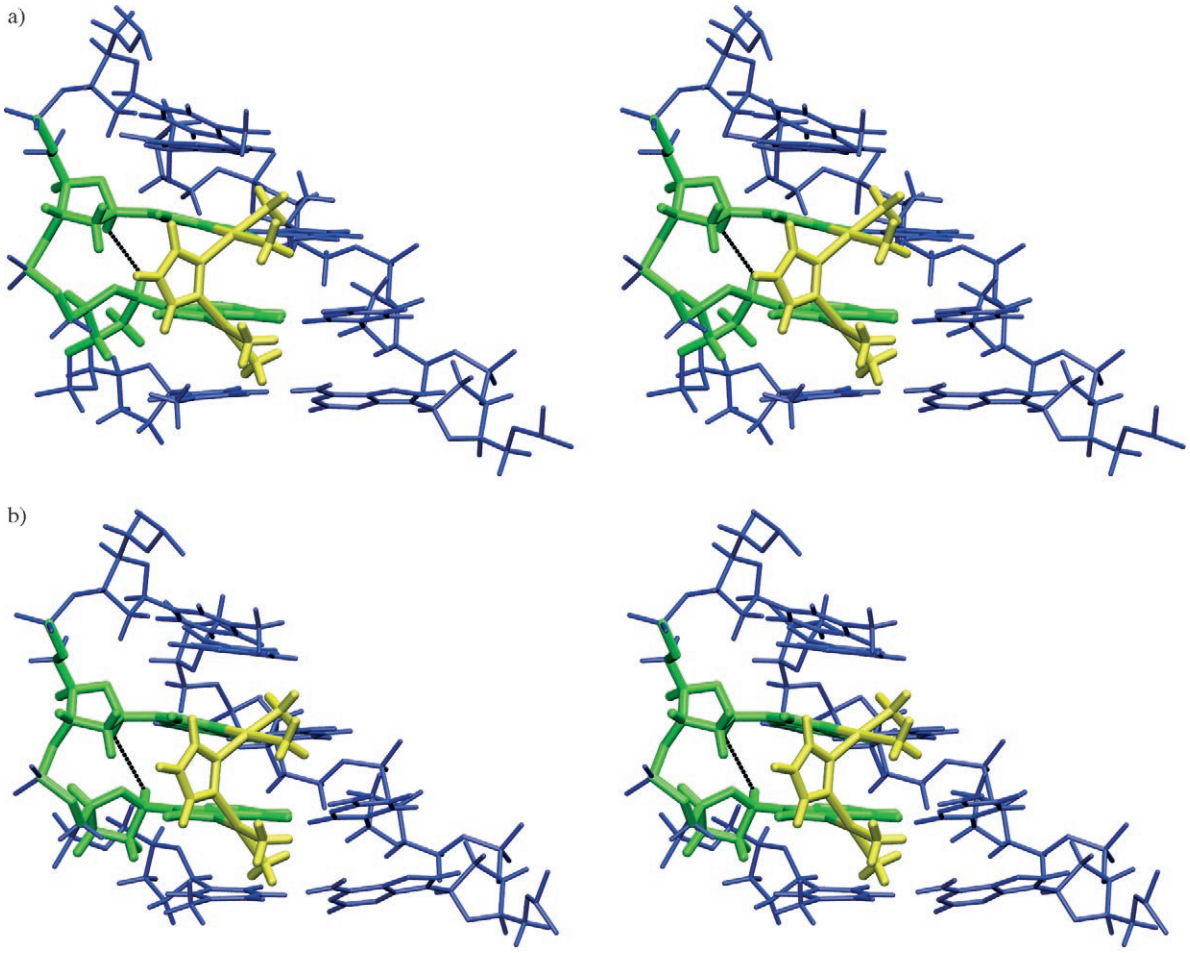

Figure 8. Stereoviews of the inner tetranucleotide d(TG*G*T)-d(ACCA) of the time-averaged models of dsII having G*6 in an N (a) and S (b) conformation, respectively. The platinated G*pG* dinucleotide is shown in green and the {*cis*-[Pt(NH_3)$_2$]}$_2$(μ-pz)$^{3+}$ residue in yellow. The G*5H1′–G*6H1′ distance is shown as a black dotted line. Its length is 2.83 Å in (a) and 3.32 Å in (b).

Table 4. Distances between the pyrazolate and guanine protons, as determined from the NOE intensities, and calculated as time-averages over the MD simulation of dsII.[a]

Distance	G*5 H8-pzH3	G*5 H8-pzH4	G*5 H8-pzH5	G*6 H8-pzH3	G*6 H8-pzH4	G*6 H8-pzH5
I_{NOE}[b]	1.75	8.38	54.9	20.2	2.75	1.6
d_{NOE} [Å][c]	4.93	3.79	2.77	3.28	4.57	5.00
d_{MD} [Å][d]	5.16(24)	4.07(18)	2.30(16)	3.31(23)	4.63(27)	5.04(27)

[a] See Figure 2 for numbering of atoms. [b] NOE intensity measured at 200-ms mixing time on an arbitrary scale. [c] Inter-proton distance determined from the NOE intensity as $d_{NOE}=(c/I_{NOE})^{1/6}$, with c set to 25000. [d] Inter-proton distance calculated as time-average over the MD simulation of dsII, with the standard deviation in parentheses.

Discussion

Chemical shifts and structure: The differences in chemical shifts between the platinated and the unplatinated duplexes contain valuable information about the three-dimensional distortions induced by the platinum complex. These differences are limited to the base-pairs involved in the platinum lesion, and are most pronounced for the aromatic protons of G*5, G*6, C15, and C16. The proximity of the pyrazole ring to protons G*5H8 and G*6H8 (Figure 8) explains, at least in part, the upfield shifts of G*5H8 ($\Delta\delta=-0.97$ ppm) and G*6H8 ($\Delta\delta=-0.18$ ppm) upon platination (see Figure 4).

Platinum coordination to the N7 atom of guanine shifts the H8 proton about 0.5 ppm downfield due to the inductive effect of Pt coordination.[31] For the H8 protons of G*5 and G*6 this effect is overcompensated by the shielding effect of the aromatic pyrazole. The fact that the compensation is much more pronounced for G*5H8 is in agreement with its position closer to the pyrazole ring.

Another effect that probably shifts the H8 resonances of G*5 and G*6 upfield is the unwinding of the duplex, which results in an increased stacking of the platinated base-pairs. This effect of increased stacking is also observed for the amino NH1/NH2 protons of C15 and C16, which are shifted upfield (by 1–1.5 ppm, Table 1) as well. These protons are positioned too far away from the pyrazole ring to experience any shielding. Weakened Watson–Crick (WC) hydrogen-bonding, which could, in principle, also cause upfield shifts, is not a likely cause here, since the upfield shift is equally observed for the WC and the non-WC protons.

Platinum binding affects the DNA conformation both by steric constraints and electronic effects: Platinum(II) forms stable and inert covalent bonds to the N7 atoms of guanines and adenines. Bifunctional, mononuclear Pt^{II} complexes, such as cisplatin, are able to cross-link two different purines; such cross-links cause strong deformations in the DNA double helix. Specifically, cisplatin cross-links of two adjacent purines bend the helix towards the major groove.[44] This bending is accompanied by repuckering of some sugar residues, most notably that of the 5′-guanosine involved in the cross-link. Such repuckering can be the consequence of a local compression of the backbone,[45] but can also have an electronic origin, since Pt-bound guanosine nucleotides intrinsically favor the N conformation, as shown already in the 1980s by some of us.[34–37] In fact, coordination of 5′-GMP to **1** has been recently shown to increase the N population in 5′-GMP.[26] In the case of the Pt-pz-Pt cross-link, the geometrical distortion of the double helix is much smaller than in the case of cisplatin cross-links; nonetheless, the NMR spectroscopic data indicate a conformational change of the 3′-guanosine towards an N-type pucker. Such a change was not observed in a control MD simulation of dsII with the unmodified parm98 force field (the force field was only supplemented by parameters defining the energetics of the Pt-pz-Pt moiety; the torsional parameters of the backbone were unchanged), thereby suggesting that the favoring of the N conformation observed for G*6 in the NMR spectra is, at least in part, of electronic origin. We have simulated this electronic effect in the work presented here by decreasing the term $V_3/2$ for the torsion angle OS–CP–CP–OS from 1.5 to 0.75 kcal mol^{-1} for platinated guanosines. Such a decrease is expected to stabilize the N conformation with respect to S.[46] In fact, this modification shifts the pucker of C*6 from purely S to an N⇌S equilibrium. Importantly, the G*5 pucker remained S even when the same modification of the force field was applied for G*5 and G*6. The structural perturbation (i.e. unwinding) caused by the Pt-pz-Pt cross-link obviously affects G*5 and G*6 unequally, and probably contributes to the S→N repuckering of G*6. The repuckering of G*6 is thus apparently caused by a combination of electronic and steric effects.

The sugar pucker of C15 (base complementary to G*6) is found to be locked in an O4′-*endo* (E) conformation. Since C15 is on the unplatinated strand the electronic effects of platination are expected to be negligible. The stable E-pucker of C15, a conformation which distinguishes this nucleotide from all other nucleotides of dsII, is therefore quite clearly a consequence of the unwinding of the double helix.

Possible implications for protein recognition: 1,2-GG cisplatin cross-links are specifically recognized by a number of minor-groove-binding proteins, such as the TATA box binding protein,[47] the *E. Coli* DNA repair recognition complex UvrAB,[48] the mismatch repair protein MutS,[49–51] or HMG box proteins.[15] By comparing several DNA–platinum adducts recognized by the chromosomal protein HMG1, Pil and Lippard have suggested that unwinding of the double helix may be an important determinant for HMG1 binding.[52] Helix unwinding widens and flattens the minor groove, and a wide and flat minor groove was indeed subsequently identified as a recognition element of several HMG box proteins.[16,53,54] Since HMG box proteins generally bend the DNA towards the major groove, and pre-bent structures, such as DNA bearing the 1,2-GG cisplatin cross-link, are recognized with high affinity by HMG proteins,[15] the bend could be also considered as a recognition element. However, the question of how the bending and unwinding must be combined to effect HMG binding is not yet clear. Figure 9 plots the depth and width of the minor groove, calculated by

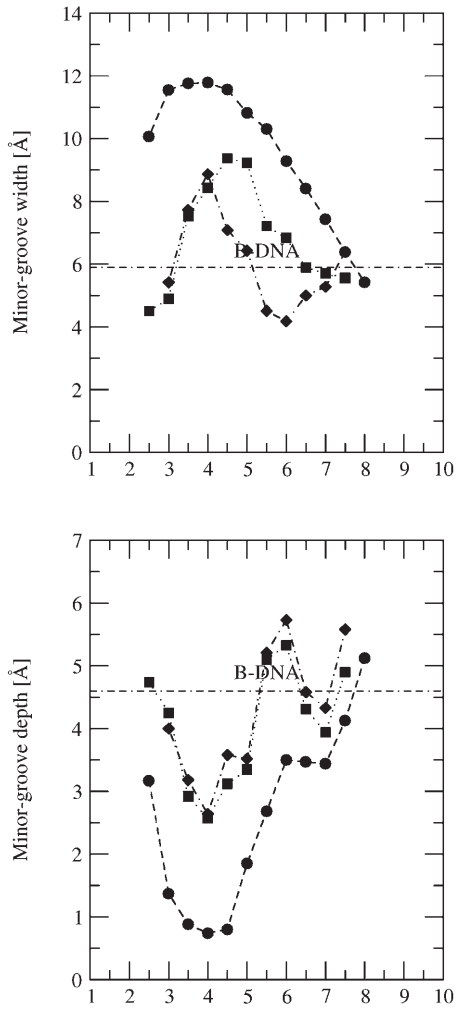

Figure 9. Width (top) and depth (bottom) of the minor groove, determined for the two energy-minimized models dsII with G*6 in an N conformation (■) and dsII with G*6 in an S conformation (◆). The all-BI model of d(GCCG*G*ATCGC)-d(GCGATCCGGC) bears a {*cis*-[Pt(NH$_3$)$_2$]}–G*G* cross-link (●).[13] Both duplexes are aligned such that nucleotides 4 and 5 correspond to the platinated G*s.

using the CURVES program,[42] for the two minimized structures of dsII (differing in the conformation of the G*6 sugar) and compares these parameters with those determined for the cisplatin–GG cross-link.[13] It can be seen that the GG cross-link by Pt-pz-Pt widens and flattens the minor groove approximately half as much as the GG–cisplatin cross-link. Thus, the Pt-pz-Pt DNA cross-link, for which dsII is a model, would be an interesting test case for HMG recognition, since it causes, as we have shown here, an unwinding of the double helix similar to that of cisplatin, but virtually no bending, and produces smaller widening and flattening of the minor groove. In addition to testing whether the Pt-pz-Pt cross-link is recognized by HMG proteins, it would also be of interest to see how the cross-link is recognized by repair proteins and polymerases. Comparing the recognition of the Pt-pz-Pt–DNA adducts with that of cisplatin adducts should provide valuable keys to the recognition mechanism, and hopefully enable the individual contributions of DNA bending and unwinding to protein recognition to be assessed.

Conclusion

The interaction of the new cytotoxic compound [(*cis*-{Pt(NH$_3$)$_2$}$_2$(μ-OH)(μ-pz)](NO$_3$)$_2$ with a decamer oligonucleotide has been studied by NMR spectroscopy and molecular modeling. The complex was designed with the aim to induce minimal distortions upon binding to adjacent guanines of DNA. We have recently shown that GG sites are favorable targets for this new drug.[55]

The present study demonstrates that the Pt-pz-Pt cross-link of two adjacent guanines indeed induces relatively minor structural perturbations upon the DNA double helix. The DNA is shown to accommodate the cross-link without significant bending or base-pair disruption. Corroborating this result, the melting temperature was found to be essentially identical to that of the unplatinated duplex.

The MD simulation indicates that the only pronounced effect of the cross-link on the global structure is an unwinding by about 15° of the step between the two platinated GC pairs. This unwinding becomes manifest in an unusual H1′–H1′ NOE between G*5 and G*6 and in strong upfield shifts of all amino protons of C15 and C16. The unwinding, in turn, affects the sugars of the G*6:C15 base-pair: that of G*6 shows rapid N–S interconversion, whereas that of C15 is locked in an E-type conformation.

The determination of the structure of the Pt-pz-Pt cross-link at two adjacent guanines was a logical and necessary step towards the elucidation of the antitumor mechanism of the new dinuclear antitumor complex [(*cis*-{Pt(NH$_3$)$_2$}$_2$(μ-OH)(μ-pz)]$^{2+}$. The fact that, similar to cisplatin, this complex cross-links two adjacent guanines of DNA, induces a similar unwinding, but does not bend the helix axis, makes it a very interesting test compound for future studies of structural determinants governing protein recognition of platinum–DNA adducts.

Finally, we note that [(*cis*-{Pt(NH$_3$)$_2$}$_2$(μ-OH)(μ-pz)](NO$_3$)$_2$ is the first successful example of a cytotoxic platinum complex that was designed to produce a specific structural distortion in DNA. It represents a promising and encouraging case of rational drug design.

Experimental Section

Platination reaction and sample preparation: The 10-mer oligonucleotide ssI [d(C1T2C3T4G5G6T7C8T9C10)] and its complement ssII [d(G20A19G18A17C16C15A14G13A12G11)] were synthesized by the phosphoramidite method. After purification by preparative anion-exchange FPLC (Pharmacia Q Sepharose column, with a linear 0–1.2-M NaCl gradient in 0.02 M NaOH, pH 12), the solution was desalted with a gel filtration column (Pharmacia, Sephadex G25, DNA grade). The purity of the oligonucleotides was assessed by analytical anion-exchange FPLC (Pharmacia, Mono Q column); a Dowex column (Sigma) was sub-

sequently used to exchange the counterion to sodium. FPLC chromatography was performed on a BioLogic HR chromatography system (BioRad).

$[(cis\text{-}\{Pt(NH_3)_2\})_2(\mu\text{-}OH)(\mu\text{-}pz)](NO_3)_2$ was synthesized as described previously[25] from $[(cis\text{-}\{Pt(NH_3)_2\}(\mu\text{-}OH))_2](NO_3)_2$ and pyrazole. The complex was allowed to react with the purine-rich oligonucleotide (ssI) (6 mg) in a 1:1 ratio in H_2O (1 mL). The pH was adjusted to 4.0 with nitric acid. The reaction was monitored over time by FPLC (Pharmacia, Mono Q column, 20 min, 0–1.2-M NaCl gradient at pH 12). After four days at ambient temperature the reaction was judged to be complete and the reaction mixture was purified by FPLC (Pharmacia Mono Q column, 20 min, 0–1.2-M NH_4HCO_3 gradient at pH 9). The platinated DNA solution was subjected to a first round of desalting by rotary evaporation, addition of water, and lyophilization. The residue was redissolved in water and further desalted with a gel filtration column (Pharmacia, Sephadex G25, DNA grade); the desired fractions were collected and lyophilized to yield 3.5 mg of the platinated single strand d(C1T2C3T4G*5G*6T7C8T9C10) (ssIII), which contains the 1,2-intrastrand (Pt-pz-Pt)–DNA cross-link.

The unplatinated duplex dsI was prepared by titrating ssII with a solution of ssI in D_2O for comparison. The annealing was carried out at ambient temperature and monitored by anion FLPC run at pH 7. The same procedure was repeated with ssII and ssIII to produce the platinated dsII. Both duplexes were lyophilized and redissolved three times in 99.8% D_2O, and finally redissolved in 99.96% D_2O (250 μL). The solutions were transferred to an NMR tube, dried in a stream of nitrogen, and redissolved in 99.96% D_2O (550 μL). For H_2O samples, dsII was dissolved in 90% H_2O/10% D_2O (550 μL). Final concentrations were 1.0 mM for dsI and 4 mM for dsII. All samples contained 50 mM phosphate buffer pH 7.0. No additional salt was added.

UV measurements and T_m determination: For concentration determination UV measurements were performed with a Perkin–Elmer Lambda 900 UV/VIS/NIR spectrometer. Melting temperatures (T_m) were measured with an Ultrospec 4000 UV spectrometer by heating the sample at 1 °C min^{-1} from 20 °C to 90 °C at oligonucleotide concentrations of 3.4×10^{-9} M in 1 M NaCl and 50 mM phosphate buffer.

NMR spectroscopy: TOCSY and NOESY spectra (mixing times of 100, 150, and 200 ms) were acquired with a Bruker DMX 600 MHz spectrometer, using the Watergate gradient pulse for minimization of the water signal.[56] All 2D spectra were collected at 283 K. 512 Increments in t_1 were collected, each with 2048 complex data points in t_2, and 64 scans at a sweep width of 6000 Hz. Spectra in H_2O were collected with a sweep width of 12000 Hz. T1 relaxation experiments were carried out using the standard 180°–τ–90° inversion recovery sequence.

All spectra were processed with FELIX (version 97.0, MSI, San Diego, CA, USA), except for the T1 relaxation experiments; these were processed with xwinNMR software (Bruker). For 2D spectra the t_1 dimension was zero-filled to 2048 points and a polynomial baseline correction was applied in the t_2 domain of the NOESY spectra. Chemical shifts were referenced to the HDO peak calibrated to a DSS (2,2-dimethyl-2-silapentane sulfonate) standard. The assignment aiding program ANSIG[57] was employed to aid assignments and to view and compare spectra of the platinated and unplatinated duplexes.

Molecular dynamics simulations: The MD simulations were carried out with the SANDER module of the program AMBER Version 6.0[58] run on a cluster of IBM-compatible personal computers under Red Hat GNU/Linux 7.1, or on an IBM Power4 P690 computer operating under AIX 5.1. The Particle–Mesh–Ewald method,[59,60] using a charge grid spacing of approximately 1 Å with cubic B-spline interpolation and sum tolerance of 10^{-5} Å, was used to calculate the electrostatic energy. A 9-Å cutoff was applied to Lennard–Jones interactions. The MD simulations employed the SHAKE algorithm (tolerance = 0.0005) to all X–H bonds[61] and used a time step of 2 fs.

Additional force field terms were necessary to parameterize the Pt-pz-Pt moiety. The bond lengths and bond angles were taken from the crystal structure of $[(cis\text{-}\{Pt(NH_3)_2\}(9\text{-ethylguanine}))_2(\mu\text{-}pz)]^{3+}$,[25] and the corresponding force constants were equivalenced to those of the five-membered ring of histidine. The same parameters were used for the Pt–N(pyrazole) bonds as for the Pt–N(guanine) bonds.[8] All endocyclic and exocyclic torsion angles not involving Pt were given energy barriers $k_d/2$ in analogy to those used by Amber for the five-membered ring of histidine. The torsion angles X-X-N-Pt that govern the out-of-plane bending of the platinum with respect to the pyrazole were parameterized as follows. First, those torsions involving a hydrogen atom (H-C-N-Pt) were given a torsion barrier of 1.1 kcal mol^{-1}, in analogy to the values used for torsions involving aromatic hydrogen atoms in the Amber database. Second, the Pt-N-N-Pt torsion was given a barrier of 0 in order to avoid biasing of the mutual positions of the two platinum centers. Thus, the principal force keeping the platinum atoms in the pyrazole plane is dependent on the torsion angles C-N-N-Pt and C-C-N-Pt. The force constant for these torsions was determined to be $k_d/2 = 40$ kcal mol^{-1} by density functional theory (DFT) calculations, as described below.

Force constants determining the dihedral angles between the pyrazole plane and the Pt coordination plane, and the atomic charges of the $[(cis\text{-}\{Pt(NH_3)_2\})_2(\mu\text{-}pz)(pGpG)]^+$ unit, were obtained from DFT calculations performed with the program Gaussian94[62] implemented on a Cray C94 computer. Starting coordinates were taken from the crystal structure of $[(cis\text{-}\{Pt(NH_3)_2\}(9\text{-ethylguanine}))_2(\mu\text{-}pz)]^{3+}$, and, to save computer time, the 9-ethyl group was replaced by a 9-methyl group. To eliminate the influence of crystal-packing forces, the geometry was relaxed by minimizing the energy as a function of the four dihedral angles along the Pt–N bonds, using Hartree–Fock (HF) calculations. Subsequent DFT calculations employing the hybrid B3LYP functional were performed on the HF-optimized geometry, using MO coefficients from the HF calculation as trial vectors. The atomic charges were determined by fits to the electrostatic potential obtained from the converged DFT density matrix, using the Merz–Kollman routine implemented in Gaussian94. Both the HF and the B3LYP calculations used the Los Alamos pseudo-potential/pseudo-orbital basis set LANL2DZ.[63] To determine the force constants governing the out-of-plane bending of the pyrazole, DFT calculations were performed on the model complex $[Pt(NH_3)_3(Hpz)]^{2+}$. The Pt–N3 bond was bent from the Pz plane in steps of 5° and the force constants were obtained by fitting the resulting calculated energies to the Amber energy function for dihedral angles.

The sugar-phosphate backbone was modified to take into account the influence of the platination upon DNA fixation on the adjacent sugar and phosphate residues:[34–38] The $V_3/2$ potential for the torsion angle O4′-C4′-C3′-O3′ was reduced from 1.50 kcal mol^{-1} to 0.75 kcal mol^{-1} and a $V_2/2$ torsion term for the dihedral angle C2′-C3′-O3′-P of 1.00 kcal mol^{-1} was introduced to mimic the stabilization of the ε^t conformation of platinated guanosines. These torsion barriers were determined from a number of test simulations of platinated oligonucleotides (S. Teletchéa, D. Djuranovic, J. Kozelka, unpublished results).

Simulation protocol: The starting structure for dsII, d(C1T2C3T4G*5G*6T7C8T9C10)-d(G20A19G18A17C16C15A14G13-A12G11) (where G*5G*6 denotes the Pt-pz-Pt cross-link) was generated using a canonical Arnott B-DNA[64] as a starting model with the program NUCGEN. The $[(cis\text{-}\{Pt(NH_3)_2\})_2(\mu\text{-}pz)]^{3+}$ residue was then manually positioned using XLEAP. The resulting DNA-chelate was minimized by 100 steps of conjugate gradient minimization. The system was then heated and equilibrated as described for the simulation protocol of Elizondo-Riojas and Kozelka.[13]

Unrestrained dynamics production was carried out for 20000 ps. The 20000 structures (one per picosecond) of the MD trajectory were analyzed by using the programs Carnal (in the Amber package), CURVES,[42] VMD,[65] XmGrace (http://plasma-gate.weizmann.ac.il/Grace/), and in-house software (http://www.steletch.org). Base–base helicoidal parameters were determined relative to the local axis, whereas for parameters relating base-pairs (Table 3), the global axis[42] was employed.

Acknowledgments

We are indebted to Dr. B. Hartmann for constructive discussions and numerous analyses of the NDB database. J.K. and S.T. thank the Associa-

tion for International Cancer Research (AICR; grant no. 00–321) and l'Association pour la Recherche contre le Cancer (A.R.C; grant P01/3/4297) for financial support. S.K is indebted to The Kidani Memorial Trust for a fellowship. Computer time from the IDRIS computer center of the CNRS and support from COST (Projects D20/001/00 and D20/003/00), enabling scientific exchange with other research groups, are gratefully acknowledged. M.-A.E.-R. received the 1997 Gemini award from the International Precious Metals Institute (IPMI). This research was financially supported in part by the Council for Chemical Sciences of the Netherlands Organization for Scientific Research (CW-NWO). The authors are grateful to Johnson Matthey (Reading, UK) for their generous loan of K_2PtCl_4.

[1] Z. Guo, P. J. Sadler, *Angew. Chem.* **1999**, *111*, 1610–1630; *Angew. Chem. Int. Ed.* **1999**, *38*, 1512–1531.
[2] P. J. O. Dwyer, J. P. Stevenson, S. W. Johnson in *Cisplatin: Chemistry and Biochemistry of a Leading Anticancer Drug* (Ed.: B. Lippert), Verlag Helvetica Chimica Acta, Zürich, **1999**, pp. 29–69.
[3] G. Chu, *J. Biol. Chem.* **1994**, *269*, 787–790.
[4] M. C. Christian, *Semin. Oncol.* **1992**, *19*, 720.
[5] J. Reedijk, *Chem. Commun.* **1996**, 801–806.
[6] J. Reedijk, *Proc. Natl. Acad. Sci. USA* **2003**, *100*, 3611–3616.
[7] A. M. J. Fichtinger-Schepman, J. L. van der Veer, J. H. J. Den Hartog, P. H. M. Lohman, J. Reedijk, *Biochemistry* **1985**, *24*, 707–713.
[8] F. Herman, J. Kozelka, V. Stoven, E. Guittet, J.-P. Girault, T. Huynh-Dinh, J. Igolen, J.-Y. Lallemand, J.-C. Chottard, *Eur. J. Biochem.* **1990**, *194*, 119–133.
[9] D. Yang, S. S. G. E. van Boom, J. Reedijk, J. H. van Boom, A. H.-J. Wang, *Biochemistry* **1995**, *34*, 12912–12920.
[10] P. M. Takahara, A. C. Rosenzweig, C. A. Frederick, S. J. Lippard, *Nature* **1995**, *377*, 649–652.
[11] A. Gelasco, S. J. Lippard, *Biochemistry* **1998**, *37*, 9230–9239.
[12] J. A. Parkinson, Y. Chen, Z. Guo, S. J. Berners-Price, T. Brown, P. J. Sadler, *Chem. Eur. J.* **2000**, *6*, 3636–3644.
[13] M.-A. Elizondo-Riojas, J. Kozelka, *J. Mol. Biol.* **2001**, *314*, 1227–1243.
[14] L. G. Marzilli, J. S. Saad, Z. Kuklenyik, K. A. Keating, Y. Xu, *J. Am. Chem. Soc.* **2001**, *123*, 2764–2770.
[15] D. B. Zamble, S. J. Lippard in *Cisplatin: Chemistry and Biochemistry of a Leading Anticancer Drug* (Ed.: B. Lippert), Verlag Helvetica Chimica Acta, Zürich, **1999**, pp. 73–110.
[16] U. M. Ohndorf, M. A. Rould, Q. He, C. O. Pabo, S. J. Lippard, *Nature* **1999**, *399*, 708–712.
[17] M. A. Fuertes, J. Castilla, C. Alonso, J. M. Pérez, *Curr. Med. Chem.* **2003**, *10*, 257–266.
[18] N. Farrell, Y. Qu, U. Bierbach, M. Valsecchi, E. Menta in *Cisplatin: Chemistry and Biochemistry of a Leading Anticancer Drug* (Ed.: B. Lippert), Verlag Helvetica Chimica Acta, Zürich, **1999**, pp. 479–521.
[19] Y. Zou, B. Van Houten, N. Farrell, *Biochemistry* **1994**, *33*, 5404–5410.
[20] Y. Qu, M. J. Bloemink, J. Reedijk, T. W. Hambley, N. Farrell, *J. Am. Chem. Soc.* **1996**, *118*, 9307–9313.
[21] D. Yang, S. S. G. E. van Boom, J. Reedijk, J. H. van Boom, N. Farrell, A. H.-J. Wang, *Nat. Struct. Biol.* **1995**, *2*, 577–586.
[22] J. Kozelka, E. Segal, C. Bois, *J. Inorg. Biochem.* **1992**, *47*, 67–80.
[23] S. Komeda, M. Lutz, A. L. Spek, M. Chikuma, J. Reedijk, *Inorg. Chem.* **2000**, *39*, 4230–4236.
[24] S. Komeda, M. Lutz, A. L. M. Spek, Y. Yamanaka, T. Sato, M. Chikuma, J. Reedijk, *J. Am. Chem. Soc.* **2002**, *124*, 4738–4746.
[25] S. Komeda, H. Ohishi, H. Yamane, M. Harikawa, K. Sakaguchi, M. Chikuma, *J. Chem. Soc. Dalton Trans.* **1999**, 2959–2962.
[26] S. Komeda, H. Yamane, M. Chikuma, J. Reedijk, *Eur. J. Inorg. Chem.* **2004**, 4828–4835.
[27] D. R. Hare, D. E. Wemmer, S.-H. Chou, G. Drobny, B. R. Reid, *J. Mol. Biol.* **1983**, *171*, 319–336.
[28] M. A. Akkerman, C. A. G. Haasnoot, C. W. Hilbers, *Eur. J. Biochem.* **1988**, *173*, 211–225.
[29] M. A. Akkerman, E. W. Nejiman, S. S. Wijmenga, C. A. G. Haasnoot, C. W. Hilbers, *J. Am. Chem. Soc.* **1990**, *112*, 7462–7474.
[30] S. S. Wijmenga, M. M. W. Mooren, C. W. Hilbers in *NMR of Macromolecules: A Practical Approach* (Ed.: G. C. K. Roberts), Oxford University Press, New York, **1993**, pp. 218–283.
[31] D. Lemaire, M.-H. Fouchet, J. Kozelka, *J. Inorg. Biochem.* **1994**, *53*, 261–271.
[32] F. J. M. van de Ven, C. W. Hilbers, *Eur. J. Biochem.* **1988**, *178*, 1–38.
[33] S. S. Wijmenga, B. N. M. van Buuren, *Prog. Nucl. Magn. Reson. Spectrosc.* **1998**, *34*, 287–387.
[34] A. T. M. Marcelis, C. G. van Kralingen, J. Reedijk, *J. Inorg. Biochem.* **1980**, *13*, 213–222.
[35] A. T. M. Marcelis, C. Erkelens, J. Reedijk, *Inorg. Chim. Acta* **1984**, *91*, 129–135.
[36] J. H. J. den Hartog, C. Altona, J. H. van Boom, A. T. M. Marcelis, L. J. Rinkel, G. Wille-Hazeleger, J. Reedijk, *Eur. J. Biochem.* **1983**, *134*, 485–495.
[37] C. J. Van Garderen, C. Altona, J. Reedijk, *Inorg. Chem.* **1990**, *29*, 1481–1487.
[38] M. Polak, J. Plavec, A. Trifonova, A. Földesi, J. Chattopadhyaya, *J. Chem. Soc. Perkin Trans. 1* **1999**, 2835–2843.
[39] C. Altona, M. Sundaralingam, *J. Am. Chem. Soc.* **1972**, *94*, 8205–8212.
[40] D. Djuranovic, B. Hartmann, *J. Biomol. Struct. Dyn.* **2003**, *21*, 771–788.
[41] R. E. Dickerson, M. Bansal, C. R. Calladine, S. Diekman, W. N. Hunter, O. Kennard, *J. Mol. Biol.* **1989**, *205*, 787–791.
[42] R. Lavery, H. Sklenar, *J. Biomol. Struct. Dyn.* **1989**, *7*, 655–667.
[43] P. Varnai, D. Djuranovic, R. Lavery, B. Hartmann, *Nucleic Acids Res.* **2002**, *30*, 5398–5406.
[44] S. O. Ano, Z. Kuklenyik, L. G. Marzilli in *Cisplatin: Chemistry and Biochemistry of a Leading Anticancer Drug* (Ed.: B. Lippert), Verlag Helvetica Chimica Acta, Zürich, **1999**, pp. 247–291.
[45] J. Kozelka, S. Archer, G. A. Petsko, S. J. Lippard, G. J. Quigley, *Biopolymers* **1987**, *26*, 1245–1271.
[46] T. E. Cheatham III, P. Cieplak, P. A. Kollman, *J. Biomol. Struct. Dyn.* **1999**, *17*, 845–862.
[47] P. Vichi, F. Coin, J.-P. Renaud, W. Vermeulen, J. H. J. Hoeijmakers, D. Moras, J.-M. Egly, *EMBO J.* **1997**, *16*, 7444–7456.
[48] R. Visse, M. de Ruijter, J. Brouwer, J. A. Brandsma, P. van de Putte, *J. Biol. Chem.* **1991**, *266*, 7609–7617.
[49] D. R. Duckett, J. T. Drummond, A. I. H. Murchie, J. T. Reardon, A. Sancar, D. M. J. Lilley, P. Modrich, *Proc. Natl. Acad. Sci. USA*, **1996**, *93*, 6443–6447.
[50] Z. Z. Zdraveski, J. A. Mello, C. K. Farinelli, J. M. Essigmann, M. G. Marinus, *J. Biol. Chem.* **2002**, *277*, 1255–1260.
[51] L. Fourrier, P. Brooks, J.-M. Malinge, *J. Biol. Chem.* **2003**, *278*, 21267–21275.
[52] P. M. Pil, S. J. Lippard, *Science* **1992**, *256,* 234–237.
[53] J. J. Love, X. Li, D. A. Case, K. Giese, R. Grosschedl, P. E. Wright, *Nature* **1995**, *376*, 791–795.
[54] M. H. Werner, J. R. Huth, A. Gronenborn, G. M. Clore, *Cell* **1995**, *81*, 705–714.
[55] S. Komeda, S. Bombard, S. Perrier, J. Reedijk, J. Kozelka, *J. Inorg. Biochem.* **2003**, *96*, 357–366.
[56] V. Sklenar, M. Piotto, R. Leppik, V. Saudek, *J. Magn. Reson. Ser. A* **1993**, *102*, 241–245.
[57] P. J. Kraulis, *J. Magn. Reson.* **1989**, *24*, 627–633.
[58] D. A. Case, D. A. Pearlman, J. W. Caldwell, T. E. Cheatham III, W. S. Ross, C. L. Simmerling, T. A. Darden, K. M. Merz, Jr., R. V. Stanton, A. L. Cheng, J. J. Vincent, M. Crowley, V. Tsui, R. J. Radmer, Y. Duan, J. Pitera, I. Massova, G. L. Seibel, U. C. Singh, P. K. Weiner, P. A. Kollman, AMBER 6, University of California, San Francisco, **1999**.
[59] T. A. Darden, D. York, L. G. Pedersen, *J. Chem. Phys.* **1993**, *98*, 10089–10092.
[60] U. Essman, L. Perera, M. Berkowitz, T. A. Darden, H. Lee, L. G. Pedersen, *J. Chem. Phys.* **1995**, *103*, 8577–8593.

[61] J. P. Ryckaert, G. Ciccotti, H. J. C. Berendsen, *J. Comput. Phys.* **1977**, *23*, 327–341.
[62] M. J. Frisch, G. W. Trucks, H. B. Schlegel, P. M. W. Gill, B. G. Johnson, M. A. Robb, J. R. Cheeseman, T. A. Keith, G. A. Petersson, J. A. Montgomery, K. Raghavachari, M. A. Al-Laham, V. G. Zakrzewski, J. V. Ortiz, J. B. Foresman, J. Cioslowski, B. B. Stefanov, A. Nanayakkara, M. Challacombe, C. Y. Peng, P. Y. Ayala, W. Chen, M. W. Wong, J. L. Andres, E. S. Replogle, R. Gomperts, R. L. Martin, D. J. Fox, J. S. Binkley, D. J. Defrees, J. Baker, J. P. Stewart, M. Head-Gordon, C. Gonzalez, J. A. Pople, GAUSSIAN 94, Revision C, 3rd ed., Gaussian, Inc., Pittsburgh, PA, USA, **1995**.
[63] P. J. Hay, W. R. Wadt, *J. Chem. Phys.* **1985**, *82*, 299–310.
[64] S. Arnott, P. Campbell-Smith, P. Chandresekharan, *CRC Handbook of Biochemistry, Vol. 2*, **1976**, pp. 411–414.
[65] A. Dalke, W. Humphrey, J. Ulrich, VMD (Visual Molecular Dynamics), edition 1.2b1, Theoretical Biophysics Group, University of Illinois and Beckman Institute, Urbana, USA, **1997**.

Received: July 31, 2005
Revised: November 2, 2005
Published online: March 3, 2006

